Journal of Physics: Photonics

OPEN ACCESS

RECEIVED
15 October 2024

REVISED
28 January 2025

ACCEPTED FOR PUBLICATION
4 February 2025

PUBLISHED
28 March 2025

PAPER

Work extraction from a controlled quantum emitter

Kavalambramalil George Paulson[1,*], **Hanna Terletska**[1] **and Herbert F Fotso**[2]

[1] Department of Physics and Astronomy, Middle Tennessee State University, Murfreesboro, TN 37132, United States of America
[2] Department of Physics, University at Buffalo SUNY, Buffalo, NY 14260, United States of America
[*] Author to whom any correspondence should be addressed.

E-mail: paulson.kavalambramalilgeorge@mtsu.edu

Keywords: quantum control, quantum emitter, quantum battery, ergotropy, light–matter interaction

Abstract

We investigate how an external driving field can control the amount of extractable work from a quantum emitter, a two-level quantum system (TLS) interacting with a photonic environment. In this scenario, the TLS functions as a quantum battery, interacting with the photonic bath that discharges it while the control field recharges it. Ergotropy serves as our measure of the extractable work from the quantum system. We systematically analyze how the ergotropy of the system evolves as it interacts with the photonic bath under the control of either a continuous driving field or a periodic pulse sequence. The coherent and incoherent contributions to the total ergotropy for various initial states are calculated. The role of detuning between the driving field and the emission frequency of the TLS, as well as the initial state of the system in work extraction, are investigated for continuous and periodic pulse-driving fields. We show that detuning has little impact on work extraction for a system driven by a periodic sequence of instantaneous pulses. However, for a continuously driven system, as the system approaches its steady state, ergotropy increases with detuning increases.

1. Introduction

The ability to precisely control and manipulate quantum systems is paramount in quantum information processing and computation. The delicate nature of quantum states necessitates sophisticated strategies to achieve desired outcomes, making the control and tuning of quantum systems a focal point of research.

Ideally, quantum information processing platforms should be isolated from their environment. However, ideal closed quantum systems are rare in nature. Most quantum systems interact with their surrounding environment, facilitating the exchange of both matter and energy. These interactions induce significant and complex alterations in the dynamics of the quantum system, often leading to decoherence and dissipation of the quantum state. This highlights the necessity of effective control techniques to regulate the environment's influence on quantum systems. Thus, successfully implementing diverse quantum architectures relies on adeptly managing this environmental impact. Various approaches have been developed to mitigate the decoherence and dissipation that arise from the system's interaction with its environment [1–3]. In the case of photon-mediated operations, manipulating the absorption and emission of a quantum system and forcing it to occur at specific frequencies is a pivotal aspect of quantum control, achieved through exposure to either a continuous laser field or a sequence of optical pulses [4–9]. Such protocols have been shown to have potentially dramatic effects on the performance of photon-mediated quantum information processing operations [9–11], making it important to investigate the impact of such control protocols on quantum emitters, as a resource for quantum information processing. Quantum batteries focus on enhancing energy storage and extraction in quantum systems [12, 13], exploiting their quantum properties. In this work, we cast the problem of controlling quantum emitters as a problem of a quantum battery. By leveraging the tools and insights from quantum information processing, we explore how the unique quantum properties of emitters, such as coherence, can be harnessed to enhance energy storage and extraction.

When a control field is applied to a quantum system, it injects additional energy into the system, consequently modifying its population dynamics and average energy. The nonunitary dynamics of

dissipation and decoherence, coupled with the control pulse, is conceptually analogous to the processes involved in the charging and discharging of a quantum battery [14–17]. A quantum battery, functioning as a quantum thermodynamic system, stores energy at energy levels, and coherence is central to energy storage and utilization. Significant research has focused on developing various quantum battery models [18–24] and evaluating their effectiveness. Various methodologies have been employed to maximize the extraction of work from these batteries, aiming to optimize their performance [25–29].

Quantum control methodologies represent potentially powerful tools for unlocking the full capabilities of quantum batteries. By precisely regulating the charging and discharging mechanisms through dynamic modification of control parameters such as pulse duration and frequency, we aim to optimize work extraction and enhance the overall performance of these systems. Hence, understanding the complexities of quantum control protocols on two-level quantum systems (TLS) is of great importance from the perspective of using them as quantum batteries.

To explore the potential of quantum control methodologies in optimizing quantum batteries, we investigate a TLS interacting with a photonic bath and subjected to external driving fields. Our work examines the potential for work extraction from this non-unitarily evolving system under different conditions and control strategies. We consider various initial states and employ continuous and periodic pulse control methods for charging them. In the first protocol, the system is continuously driven by a strong driving field, while the second protocol involves applying a periodic pulse sequence. In both scenarios, we examine how the amount of extractable work from the system varies and how it is connected to the population dynamics of the TLS. In this analysis, we primarily consider two initial states for the quantum battery: the excited state with zero coherence (incoherent state) and the maximally coherent state. The (in)coherent contributions to the total ergotropy are calculated for both initial states of the quantum battery. Additionally, we examine how the detuning between the driving field frequency and the TLS natural emission frequency influences the ergotropy under the effect of either a continuous field or a periodic pulse sequence drive. Furthermore, we analyze the dynamics of coherence and its role in shaping the behavior of ergotropy, providing insights into the interplay between coherence and work extraction in different driving regimes.

This paper is organized as follows: The model of the system of a TLS interacting with a photonic bath driven by the control field is presented in section 2. In section 3, we present the theoretical formalism, including a discussion of ergotropy to quantify the amount of extractable work from the system. This section also presents the calculations of both the coherent and the incoherent contributions to the ergotropy. In section 4, we present the results for different driving protocols used for charging the quantum battery. We estimate the ergotropy of various quantum states under different driving pulses and establish its connection with population dynamics. Finally, we conclude our findings in section 5.

2. Model of a two-level quantum system coupled to the photonic bath

We consider a two-level quantum system (TLS) with the ground state $|g\rangle$ and excited state $|e\rangle$ separated with an energy $\omega_1 = \omega_0 + \Delta$, with Δ being a static detuning between the pulse carrier frequency and the TLS (as shown in figure 1). The Hamiltonian of the TLS interacting with a photonic bath, assumming bath initially in the vacuum state, within the rotating wave approximation (RWA), with all frequencies measured in the frame rotating at the frequency ω_0, is given by [7, 30]

$$H = \sum_k \omega_k a_k^\dagger a_k + \frac{\Delta}{2}\sigma_z - i\sum_k g_k\left(a_k\sigma_+ - a_k^\dagger\sigma_-\right) + \frac{\Omega_x(t)}{2}\left(\sigma_+ + \sigma_-\right), \tag{1}$$

here a_k ($a_k^\dagger$) represents the annihilation (creation) operator for the kth photon mode, ω_k is the frequency of mode k, g_k denotes the kth photon mode coupling strength with the system of consideration; and the Pauli operators of the form $\sigma_z = |e\rangle\langle e| - |g\rangle\langle g|$, $\sigma_+ = |e\rangle\langle g|$, and $\sigma_- = |g\rangle\langle e|$. The TLS is driven by a control laser field with the control pulse Rabi frequency $\Omega_x(t)$, applied at appropriate times.

We study the time-dependent dynamics of such a driven TLS by solving the master equations (within the Markovian regime, employing the RWA) of the form [30, 31]:

$$\dot{\rho} = -\frac{i}{\hbar}[H_0, \rho] + \Gamma\left(\sigma_-\rho\sigma_+ - \frac{1}{2}\{\sigma_+\sigma_-, \rho\}\right), \tag{2}$$

here the first term of the equation (2) represents the unitary part of the dynamics generated by the Hamiltonian $H_0 = \frac{\Delta}{2}\sigma_z + \frac{\Omega_x(t)}{2}(\sigma_+ + \sigma_-)$; $\{x, y\} = xy + yx$ is the anticommutator.

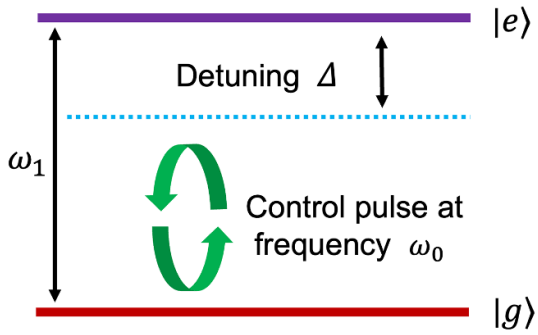

Figure 1. A schematic diagram depicting a two-level quantum system (TLS) with its ground state denoted as $|g\rangle$ and the excited state as $|e\rangle$. The detuning Δ signifies the offset between the carrier frequency ω_0 and the transition frequency ω_1 of the TLS.

Starting from the initial state of the density-matrix operator with $\rho(t=0)=\rho_{ee}(0)|e\rangle\langle e|+\rho_{gg}(0)|g\rangle\langle g|+\rho_{eg}(0)|e\rangle\langle g|+\rho_{ge}(0)|g\rangle\langle e|$ and setting $\hbar=1$, we obtain the master equations determining the time evolution of the density matrix operator for the driven quantum emitter in the form [6, 7]:

$$\begin{aligned}
\dot{\rho}_{ee} &= i\frac{\Omega_x(t)}{2}\left(\rho_{eg}-\rho_{ge}\right)-\Gamma\rho_{ee}\\
\dot{\rho}_{gg} &= -i\frac{\Omega_x(t)}{2}\left(\rho_{eg}-\rho_{ge}\right)+\Gamma\rho_{ee}\\
\dot{\rho}_{ge} &= \left(i\Delta-\frac{\Gamma}{2}\right)\rho_{ge}-i\frac{\Omega_x(t)}{2}\left(\rho_{ee}-\rho_{gg}\right)\\
\dot{\rho}_{eg} &= \left(-i\Delta-\frac{\Gamma}{2}\right)\rho_{eg}+i\frac{\Omega_x(t)}{2}\left(\rho_{ee}-\rho_{gg}\right).
\end{aligned} \tag{3}$$

As shown in [6, 7], the above master equations are obtained under a standard set of assumptions typically satisfied in experiments and calculations. This includes (a) the applicability of the Markov approximation for the emitter density matrix, implying that the electromagnetic radiation bath is not strongly perturbed by emission and/or returns to its equilibrium state quickly, and (b) the applicability of the rotating-wave approximation. The validity of these approximations was rigorously verified in [6] through benchmarking against a time-dependent density matrix renormalization group (tDMRG) study of an equivalent semi-infinite chain.

In the absence of control ($\Omega_x(t)\equiv 0$), the system exhibits spontaneous decay and the corresponding emission rate is $\Gamma=2\pi\int g_k^2\delta(\omega_k-\omega_1)\mathrm{d}k$. For the case of a continuously driven system, the Rabi frequency remains constant over time $\Omega_x(t)=\Omega$. In the controlled case, a square-shaped pulse is considered for $\Omega_x(t)=\Omega$ during the pulse's active period and remains zero otherwise.

In the following, the energy and time units are normalized by setting $\Gamma=2$, and the corresponding spontaneous emission line has a simple Lorentzian shape with half-width equal to 1. In this manuscript, all energies and times are expressed in units of Γ and $1/\Gamma$, respectively.

The assumption of a strong and brief pulse driving ($\Omega\gg\Delta,\Gamma$) is adopted, enabling us to treat the pulses as instantaneous. For instance, the application of π_x pulses inverts the population of excited and ground states and swaps the values of the coherence terms ρ_{eg} and ρ_{ge} as

$$\rho(n\tau+0)=\sigma_x\rho(n\tau-0)\sigma_x, \tag{4}$$

where $\rho(n\tau-0)$ and $\rho(n\tau+0)$ are density matrices immediately before and after the pulse application; τ is the period of the pulse sequence, n is an integer, and $\sigma_x=|g\rangle\langle e|+|e\rangle\langle g|$, i.e. the pulses interchange ρ_{ee} with ρ_{gg}, and ρ_{eg} with ρ_{ge}.

The evolution of the TLS in the presence of a driving field represents a quantum battery-charger problem. Here, the 'battery discharge', represented by the relaxation from the excited state to the ground state of the TLS, occurs through its interaction with the photonic bath. At the same time, the driving field assumes the role of the charger, supplying energy to the system. In our analysis, we consider two initial states for the battery: the excited state with $\rho=|e\rangle\langle e|$ and the maximally coherent state with $\rho=\frac{1}{2}(|e\rangle\langle e|+|g\rangle\langle g|+|e\rangle\langle g|+|g\rangle\langle e|)$. The charging-discharging processes for these initial states of the TLS for continuously driven and instantaneous pulse-driven scenarios (charging protocols) are examined in section 4.

3. Method: ergotropy as a measure of the extraction of work

Ergotropy is the maximum amount of extractable work from a quantum battery using optimal cyclic transformation [32–35]. A general Hamiltonian of the quantum battery-charger model can be written as

$$\mathscr{H}(t) = \mathscr{H}_{\mathcal{B}} + \mathscr{H}_{\mathcal{C}} + \mathscr{E}(t), \tag{5}$$

where battery and charger parts are characterised by local Hamiltonians $\mathscr{H}_{\mathcal{B}}$ and $\mathscr{H}_{\mathcal{C}}$, respectively. $\mathscr{E}(t)$ is the charging operator that encompasses all terms responsible for regulating energy input, including interactions between the battery and the charger or any external driving fields.

Initially, at $t = 0$, the state of the battery-charger system is $\rho_{\mathcal{BC}}(0)$, and its evolved state at time t is denoted by $\rho_{\mathcal{BC}}(t)$. The evolved state of the battery is obtained as $\rho_{\mathcal{B}}(t) = \mathrm{Tr}_{\mathcal{C}}[\rho_{\mathcal{BC}}(t)]$. The maximum amount of total extractable work (ergotropy) from the state $\rho_{\mathcal{B}}(t)$ can be calculated using the optimal unitary cyclic transformation [32]

$$\mathrm{W}(\rho_{\mathcal{B}}(t), \mathscr{H}_{\mathcal{B}}) = \max_{U \in \mathcal{U}_{\mathrm{cf}}} \left[E(\rho_{\mathcal{B}}(t)) - E\left(U \rho_{\mathcal{B}}(t) U^{\dagger}\right)\right], \tag{6}$$

$\mathcal{U}_{\mathrm{cf}}$ represents a set of all cyclic unitary transformations. A closed-form expression for ergotropy $\mathrm{W}(\rho_{\mathcal{B}})$ of a state $\rho_{\mathcal{B}}$ can be calculated by identifying the passive state $\tilde{\rho}_{\mathcal{B}}$ with zero ergotropy, as follows

$$\mathrm{W}(\rho_{\mathcal{B}}) = E(\rho_{\mathcal{B}}) - E(\tilde{\rho}_{\mathcal{B}}), \tag{7}$$

where $E(\rho_{\mathcal{B}}) = \mathrm{Tr}(\rho_{\mathcal{B}} \mathscr{H}_{\mathcal{B}})$ is the average energy of the state $\rho_{\mathcal{B}}$. The passive state $\tilde{\rho}_{\mathcal{B}} = \sum_n r_n |\epsilon_n\rangle\langle\epsilon_n|$ with $\rho_{\mathcal{B}} = \sum_n r_n |r_n\rangle\langle r_n|$ and $\mathscr{H}_{\mathcal{B}} = \sum_n \epsilon_n |\epsilon_n\rangle\langle\epsilon_n|$, with eigenvalues of $\rho_{\mathcal{B}}$ and $\mathscr{H}_{\mathcal{B}}$ respectively, $r_0 \geqslant r_1 \geqslant \ldots . r_n$ and $\epsilon_0 \leqslant \epsilon_1 \leqslant \ldots . \epsilon_1$. The average energy of passive state, given by $E(\tilde{\rho}_{\mathcal{B}}) = \sum_n r_n \epsilon_n$.

It has been shown in [33, 34] that the quantum ergotropy of the battery can be divided into two fundamentally separate components: W_{IC}, the incoherent ergotropy and W_{C}, the coherent component of the ergotropy so that

$$\mathrm{W}(\rho_{\mathcal{B}}) = \mathrm{W}_{\mathrm{IC}}(\rho_{\mathcal{B}}) + \mathrm{W}_{\mathrm{C}}(\rho_{\mathcal{B}}). \tag{8}$$

The incoherent ergotropy $\mathrm{W}_{\mathrm{IC}}(\rho_{\mathcal{B}})$ presents the maximum work that can be extracted from the $\rho_{\mathcal{B}}$ without changing its coherence and is given as

$$\mathrm{W}_{\mathrm{IC}}(\rho_{\mathcal{B}}) = \mathrm{Tr}\left[(\rho_{\mathcal{B}} - \pi)\mathscr{H}_{\mathcal{B}}\right], \tag{9}$$

here π is the coherence-invariant state of $\rho_{\mathcal{B}}$ with a lesser average energy such that

$$\mathrm{Tr}\left[\pi \mathscr{H}_{\mathcal{B}}\right] = \min_{U_i \in U} \mathrm{Tr}\left[U_i \rho U_i^{\dagger} \mathscr{H}_{\mathcal{B}}\right], \tag{10}$$

where U is the set of unitary operators on $\rho_{\mathcal{B}}$ that preserves the coherence but lessens the average energy.

Another approach to determine the incoherent contribution to ergotropy [33] is to define W_{IC} as the utmost work retrievable from $\rho_{\mathcal{B}}$ after eliminating all its coherences using the dephasing map $\mathcal{M}_d$ such that

$$\mathrm{W}_{\mathrm{IC}}(\rho_{\mathcal{B}}) \equiv \mathrm{W}(\mathcal{M}_d(\rho_{\mathcal{B}})) = \mathrm{W}\left(\rho_{\mathcal{B}}^d\right) = \mathrm{Tr}\left(\mathscr{H}_{\mathcal{B}}\left(\rho_{\mathcal{B}}^d - \rho_{\mathcal{B}p}^d\right)\right), \tag{11}$$

here $\rho_{\mathcal{B}}^d$ has the same population as $\rho_{\mathcal{B}}$ but zero coherence. $\rho_{\mathcal{B}p}^d$ is the passive state corresponding to $\rho_{\mathcal{B}}^d$, and is obtained from $\rho_{\mathcal{B}}^d$ after rearranging the population in the descending order. The coherent contribution to entropy is obtained as follows

$$\mathrm{W}_{\mathrm{C}}(\rho_{\mathcal{B}}) = \mathrm{W}(\rho_{\mathcal{B}}) - \mathrm{W}_{\mathrm{IC}}(\rho_{\mathcal{B}}). \tag{12}$$

4. Results

This section presents our results for the coherent and incoherent contributions to the total ergotropy obtained for the TLS model. We analyze the ergotropy dynamics for different initial states under both continuous and pulse-driven charging protocols. Specifically, we consider two distinct initial states of the TLS during the charging-discharging cycles: (i) the system is initially excited, $|e\rangle$, which possesses maximum initial energy, and (ii) the system is initially in the maximally coherent state, $\frac{1}{\sqrt{2}}(|e\rangle + |g\rangle)$, characterized by maximum coherence. These states serve as representative cases for two important classes of TLS states. We estimate both coherent and incoherent contributions to the total ergotropy for each initial state. To achieve this, we explore the dynamics of work extraction under continuous and periodically driven charging strategies, providing insight into the role of initial conditions and how control fields influence the efficiency of energy extraction.

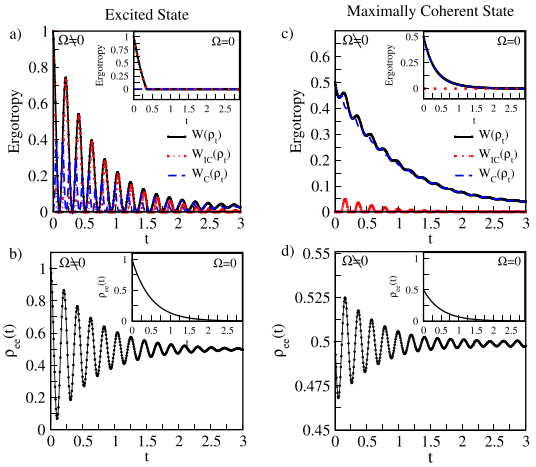

Figure 2. Variation of total ergotropy (W), incoherent and coherent ergotropy (W_{IC}, W_C), and population dynamics (ρ_{ee}) for two initial states: the excited state (left panels: (a) and (b) and the maximally coherent state (right panels: (c) and (d). The system interacts with a photonic bath driven by a field with Rabi frequency $\Omega = 30$ in the resonance regime ($\Delta = 0$). Insets display the corresponding quantities without the external control field ($\Omega = 0$). All energies and times are expressed in units of Γ and $1/\Gamma$, respectively.

4.1. Work extraction from a continuously driven TLS

We begin our analysis by exploring the behaviour of a continuously driven quantum emitter under finite Rabi oscillation ($\Omega = 30$) in the resonance regime ($\Delta = 0$). Figure 2 displays the time evolution of total ergotropy (W), coherent ergotropy (W_C), incoherent ergotropy (W_{IC}), and the excited state population (ρ_{ee}). The left panel illustrates these dynamics for the fully excited initial state ($|e\rangle$), while the right panel shows the behaviour for the maximally coherent initial state ($\frac{1}{\sqrt{2}}(|e\rangle + |g\rangle)$). The insets show the corresponding results for the non-driven case ($\Omega = 0$).

When the control field is applied ($\Omega \neq 0$), energy is injected into the TLS, akin to a charging process in a quantum battery. Dissipation and decoherence of the system result from its interaction with the photonic bath, leading to energy discharge from the system. The variation in the work extraction of a continuously driven TLS illustrates the charging-discharging process of a quantum battery. For the excited initial state shown in figures 2(a) and (b), such a charging-discharging cycle of the quantum battery follows the population dynamics, this is seen by the oscillating behaviour of the ergotropy (W) which resembles the dynamics of the excited state population ρ_{ee}. As seen in figure 2(a), both coherent and incoherent components contribute significantly to the total ergotropy. The incoherent part W_{IC} shows oscillatory behaviour, vanishes for some time, as its excited-state population decreases below the steady-state population, then revives back, and gradually diminishes as the system approaches the steady state. The coherent ergotropy W_C initially exhibits large amplitudes, but these amplitudes diminish as the state approaches the steady state, with fluctuations occurring around lower values.

Similarly, in figures 2(c) and (d), we show the ergotropy (W) and population dynamics (ρ_{ee}) for the maximally coherent initial state. As can be seen from figure 2(c), there is a little incoherent contribution (W_{IC}) to the total work extraction in the early stages of the dynamics, and the incoherent ergotropy vanishes as the excited state population decreases below its steady state, and revives back, W_{IC} later vanishes as the system approaches the steady state. In such a maximally coherent state, coherence is the main contributor to total ergotropy, evident by the dominant contribution of W_C to the total ergotropy. We also observe that unlike in the excited initial state, for the coherent case, the oscillatory nature of ergotropy W is less pronounced, which is also reflected in the population dynamics (figure 2(d)) oscillating with smaller amplitude.

To highlight the influence of the driving field on the system's evolution, the insets present the corresponding results for the non-driven case ($\Omega = 0$). In the absence of an external control field, the excited state population evolves as $\rho_{ee}(0)e^{-\Gamma t}$. For our initial excited and coherent states, $\rho_{ee}(0)$ takes the values 1 and $\frac{1}{2}$, respectively, which decay exponentially with time, as shown in figures 2(b)–(d) insets. Unlike the driven case with the oscillating behavior, the work extraction dynamics of an initial TLS state without any control field resembles the discharging process of a quantum battery without any intermediate charging methods (figures 2(a) and (c) insets). For the fully excited state, the coherent ergotropy (W_C) contribution to the total ergotropy W is zero. In contrast, for the maximally coherent initial state, the incoherent part W_{IC} does not contribute to the total ergotropy.

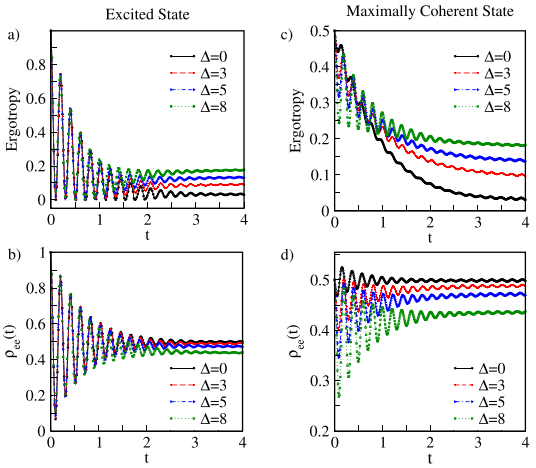

Figure 3. Time-dependent dynamics of the total ergotropy (W) and the excited state population (ρ_{ee}) for different initial conditions and values of detuning (Δ). The left panels (a) and (b) show the dynamics for an initial excited state, while the right panels (c) and (d) represent the dynamics for a maximally coherent initial state. The system is driven by a field with Rabi frequency $\Omega = 30$.

Next, we consider the influence of detuning Δ on the variation of ergotropy W. Our results for the total ergotropy W and the corresponding excited state population dynamics ρ_{ee} for different values of detuning $\Delta = 0, 3, 5, 8$ for the fully excited initial state (left panel) and maximally coherent initial states (right panel) are shown in figure 3. We show that ergotropy from the continuously driven TLS increases as the value of Δ increases for both excited and coherent states (figures 3(a) and (c)) as the system approaches steady-state dynamics. For the system initially in the excited state, from figure 3(a), it is evident that the ergotropy as a function of time increases as the detuning increases. However, this is different in the case of the maximally coherent state. For the maximally coherent state (figure 3(a), the dependence of ergotropy on detuning follows a reverse order at the early stage of the dynamics due to the difference in the (in)coherent ergotropy contribution to the total ergotropy. However, this changes as the system approaches steady state dynamics, where the ergotropy increases as Δ increases. In the left panel (a), the system initially in the excited state exhibits more pronounced oscillations, which diminish in amplitude as the steady state approaches. For the system initially in the coherent state (right panel (c)), the ergotropy in the early stage shows oscillatory behaviour for higher values of detuning Δ. As the system approaches its steady state, the oscillation of ergotropy decreases in amplitude, revealing a more pronounced dependence on Δ. Panels (b) and (d) show the corresponding population dynamics of the excited state, where similar oscillations are observed for both initial states. However, the population dynamics of the maximally coherent state (panel (d)) fluctuate between lower values, and the oscillations are less prominent compared to those of the excited state (panel (b)). The effect of detuning Δ is evident in all panels, with higher detuning (Δ) leading to a slower decay in ergotropy and a shift in population dynamics. Overall, the figure highlights that detuning Δ can be used to manipulate the ergotropy one can extract from the TLS battery over time.

To further explore the behavior of ergotropy, we investigate how coherence influences its dynamics. For a given reference basis i, a density matrix can be expressed as $\rho = \sum_{i,j} \rho_{ij} |i\rangle\langle j|$, while the incoherent density matrix-diagonal in the basis i-is written as $\rho = \sum_i \rho_i |i\rangle\langle i|$. We use the l_1 measure of quantum coherence ($C_{l_1}(\rho)$), defined as the sum of the absolute values of the off-diagonal elements [36]:

$$C_{l_1}(\rho) = \sum_{i \neq j} |\rho_{ij}|. \tag{13}$$

Our results for the calculated coherence are shown in figure 4, which depicts the coherence dynamics for the initially excited state (left panel) and the maximally coherent state (right panel) under varying detuning values, Δ. The initial coherence of the excited state is zero, whereas the maximally coherent state starts with the maximum possible coherence value of 1. As shown in the figure, the measure of coherence increases with detuning Δ, becoming particularly pronounced as the system approaches the steady state. These coherence dynamics provide valuable insights into the behavior of ergotropy during this process. Specifically, the increase in ergotropy at higher detuning values is closely related to elevated coherence levels, as observed in figures 3(a) and (c).

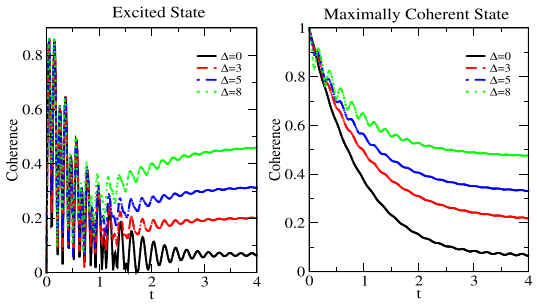

Figure 4. The dynamics of l_1 measure of coherence ($C_{l_1}(\rho)$) for different initial conditions and values of detuning $\Delta = 0, 3, 5, 8$. The left panel shows the dynamics for an initial excited state, while the right panel represents the dynamics for a maximally coherent initial state. The system is driven by a field with Rabi frequency $\Omega = 30$.

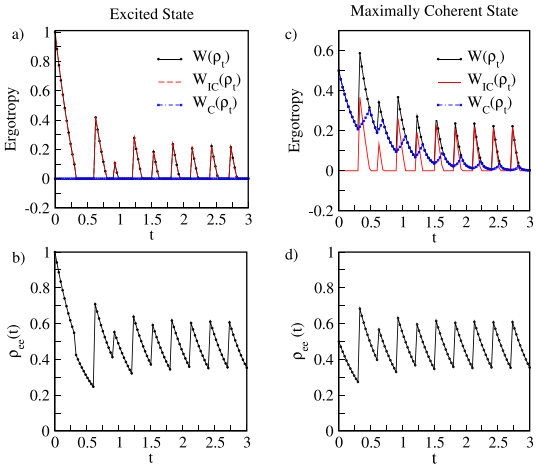

Figure 5. Variation of total ergotropy W, incoherent W_{IC}, and coherent ergotropy W_C, along with the population dynamics (ρ_{ee}) for the initially excited state (left panels) and the maximally coherent state (right panels). The system interacts with a photonic bath driven by instantaneous π_x pulses with a $\tau = 0.3$ period. Number of pulses $N_{\text{pulse}} = 10$, $\Delta = 0$.

4.2. Work extraction from a periodically-driven TLS

In this section, we analyze the work extraction from a quantum emitter driven by a periodic sequence of π_x pulses, which act as a control mechanism applied instantaneously-similar to the instantaneous charging of a quantum battery. Following each pulse, the battery discharges according to Markovian dynamics. Each π_x pulse swaps the populations of the excited and ground states while exchanging their coherence values, repeating at intervals of τ.

Figure 5 shows the discharge dynamics of the quantum battery for two initial states in the resonance regime ($\Delta = 0$), highlighting how the ergotropy and population dynamics evolve under the influence of a periodic sequence of π_x pulses and emphasizing the differences between the initial excited or maximally coherent states. For the initial excited state (left panel, figure 5(a) and (b), the π_x pulses applied periodically at a time interval $\tau = 0.3$ result in the total ergotropy decaying monotonically for one inter-pulse time interval and then vanishing for the following one. Here, the total ergotropy W consists solely of the incoherent part W_{IC}, with no contribution from coherence, as shown by the zero value of W_C. The population dynamics of the excited state (ρ_{ee}) exhibit a sharp, step-like decrease with each pulse, inverting the population between the excited and ground states. The total ergotropy vanishes as the excited-state population decreases below the steady-state population. For the maximally coherent initial state (figures 5(c) and (d), both the coherent W_C and incoherent W_{IC} components contribute to the total ergotropy W. The coherent ergotropy plays a significant role alongside the incoherent ergotropy, which diminishes as the excited state population decreases below the steady state population, resulting in oscillatory behaviour in the total extractable work. The interplay between these contributions is evident from the population dynamics in (figure 5(d))), where the periodic π_x pulses drive oscillations between the excited and ground states. The dynamics of the incoherent ergotropy are closely tied to these population oscillations, offering insight into how the population inversion impacts the extractable work from the system.

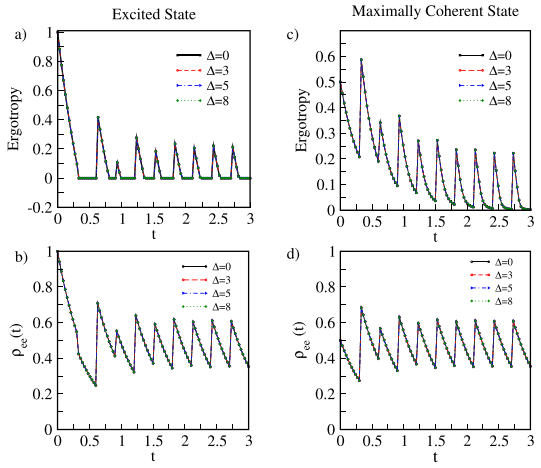

Figure 6. Variation of total ergotropy W and the population dynamics ρ_{ee} of the initially excited state (left panels) and the maximally coherent state (right panels), interacting with a photonic bath driven by instantaneous π_x pulses with a period of $\tau = 0.3$. Number of pulses $N_{\text{pulse}} = 10$, values of detuning $\Delta = 0, 3, 5, 8$.

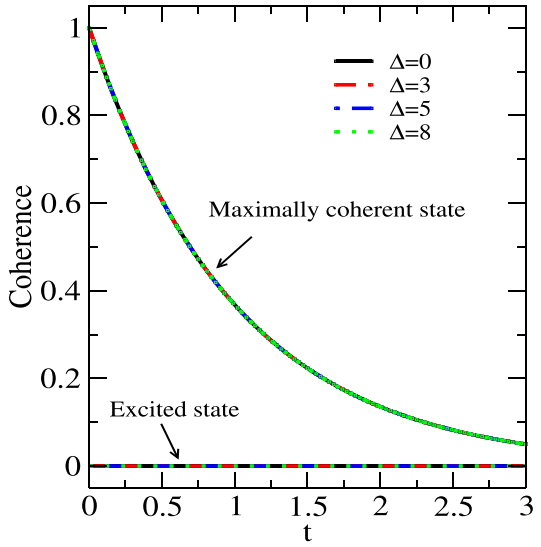

Figure 7. The l_1 measure of coherence ($C_{l_1}(\rho)$) for different initial conditions and values of detuning $\Delta = 0, 3, 5, 8$. TLS is interacting with a photonic bath driven by instantaneous π_x pulses with a period of $\tau = 0.3$. Number of pulses $N_{\text{pulse}} = 10$, values of detuning $\Delta = 0, 3, 5, 8$.

In figure 6, we investigate the effect of detuning on work extraction in a TLS driven by a periodic sequence of instantaneous π_x pulses. Unlike the case for a continuously driven system in the previous section, the detuning does not significantly alter the charging-discharging behaviour for either initial state. Each π_x pulse injects energy into the system instantaneously, acting like a rapid charge to a quantum battery, followed by a discharge phase before the next pulse is applied. We also examined the case of a finite-duration pulse (results not shown) and observed behaviour similar to that of a continuously driven system. When a finite-duration π pulse is applied for time $\frac{\pi}{\Omega}$, the effect of detuning on ergotropy is noticeable for smaller Rabi frequencies, especially in the near-resonant regime.

To investigate the effect of coherence on ergotropy in the case of an instantaneous pulse-driven system, we again examine the l_1 norm of coherence for the two initial states. Our results are shown in figure 7, where we present the behavior of coherence for the initial excited and maximally coherent states. For the system initially in the excited state, coherence remains zero throughout the evolution, and so does the coherent ergotropy (figure 5(a)). In contrast, for the system initially in the maximally coherent state ($C_{l_1}(\rho) = 1$), the instantaneous pulse modifies the off-diagonal elements by swapping them but does not alter the overall coherence. As we can see, unlike continuously driven systems (figure 4), the detuning Δ does not influence the dynamics of coherence or ergotropy in an instantaneous pulse-driven system.

5. Conclusion

In this work, we explored how a controlled two-level quantum system can serve as a model for a quantum battery when interacting with a photonic bath. We systematically analyzed work extraction under continuous field and pulse protocols, using ergotropy to quantify the extractable work. Our investigation considered two initial states of the TLS—a fully excited and a maximally coherent initial state—to explore their respective influences on the charging dynamics. We also examined the coherent and incoherent contributions to the ergotropy, finding that the nature of these contributions depends on the initial state.

For a continuously driven quantum emitter, our results demonstrate that total ergotropy increases with detuning, particularly in the near-resonant regime, where higher detuning yields greater extractable work. This behavior is closely related to the underlying dynamics of coherence. Our results remain valid across different parametric regimes. In the case of periodic π_x pulse-driven charging, we find that detuning has a negligible effect on ergotropy dynamics, in contrast to the continuous driving scenario. Instead, work extraction is primarily governed by the inter-pulse delay τ, with a change in pulse delay defining the peaks in ergotropy.

Overall, our findings underscore the importance of both the control strategy and the initial state in maximizing work extraction from a quantum battery. By systematically analyzing how various parameters affect ergotropy dynamics, our work provides insights into the operation of efficient quantum batteries and highlights the role of control protocols in optimizing energy storage and retrieval in quantum systems.

This relevance is further emphasized by recent experimental work reported in [13], which investigated the extraction of work in a single spin system. Using a solid-state qubit formed by the single electron spin of a nitrogen-vacancy center in a diamond crystal, the authors demonstrated how coherence enhances the work extraction of a quantum system. This experimental realization of coherent ergotropy in a single spin system aligns with our findings, as it highlights the capacity to extract work from various quantum battery states under different charging protocols. Moreover, the role of detuning in work extraction, as explored in our study, underscores the significance of coherence in energy storage and retrieval, offering valuable insights for nanodevice engineering and the development of quantum technologies.

Data availability statement

The data cannot be made publicly available upon publication because they are not available in a format that is sufficiently accessible or reusable by other researchers. The data that support the findings of this study are available upon reasonable request from the authors.

Acknowledgment

KGP and HT are supported by the National Science Foundation under Grant No. QIS-2328752. HT is also supported by the National Science Foundation under Grant No. DMR-1944974. HFF is supported by the National Science Foundation under Grant Nos. PHY-2014023 and QIS-2328752.

Appendix. Ergotropy calculation for a single qubit state

Consider the qubit's state,

$$\rho = \frac{1}{2}\left(\sigma_0 + r_1\sigma_x + r_2\sigma_y + r_3\sigma_z\right), \tag{A.1}$$

where $\sigma_{i=1,2,3}$ are the Pauli's spin matrix and σ_0 the identity matrix. Consider the the Hamiltonian of the form $H = \frac{\omega_0}{2}(\sigma_0 + \sigma_z)$ on the qubit state. We calculate the ergotropy of the state using equation (7)

$$\mathrm{W}(\rho) = \frac{\omega_0}{2}(r + r_3), \tag{A.2}$$

and $r = \sqrt{r_1^2 + r_2^2 + r_3^2}$. Using equation (11), we calculate the incoherent ergotropy. We have the diagonal density matrix $\rho^d = \frac{(1+r_3)}{2}|1\rangle\langle 1| + \frac{(1-r_3)}{2}|0\rangle\langle 0|$, $|1\rangle = (1,0)^{\mathrm{T}}$ and $|0\rangle = (0,1)^{\mathrm{T}}$. The Eigenvalues of ρ^d in decreasing order are $\frac{1-r_3}{2} \geqslant \frac{1+r_3}{2}$ for $-1 \leqslant r_3 \leqslant 0$, and $\frac{1+r_3}{2} \geqslant \frac{1-r_3}{2}$ for $0 < r_3 \leqslant 1$. We calculate the passive state ρ_p^d as $\frac{(1+r_3)}{2}|1\rangle\langle 1| + \frac{(1-r_3)}{2}|0\rangle\langle 0|$ and $\frac{(1-r_3)}{2}|1\rangle\langle 1| + \frac{(1+r_3)}{2}|0\rangle\langle 0|$ for the intervals $-1 \leqslant r_3 \leqslant 0$ and $0 < r_3 \leqslant 1$, respectively. The incoherent ergotropy for the quantum state ρ are 0 and $r_3\omega_0$, for $-1 \leqslant r_3 \leqslant 0$, and $0 < r_3 \leqslant 1$, respectively. The coherent contribution to the ergotropy for the two previously considered intervals of r_3 is calculated as $\frac{\omega_0}{2}(r + r_3)$ and $\frac{\omega_0}{2}(r - r_3)$.

ORCID iD

Kavalambramalil George Paulson https://orcid.org/0000-0002-6156-1106

References

[1] Viola L and Lloyd S 1998 *Phys. Rev.* A **58** 2733
[2] Shiokawa K and Lidar D 2004 *Phys. Rev.* A **69** 030302
[3] Kuopanportti P, Möttönen M, Bergholm V, Saira O-P, Zhang J and Whaley K B 2008 *Phys. Rev.* A **77** 032334
[4] Patel R B, Bennett A J, Farrer I, Nicoll C A, Ritchie D A and Shields A J 2010 *Nat. Photon.* **4** 632
[5] Gao W, Imamoglu A, Bernien H and Hanson R 2015 *Nat. Photon.* **9** 363
[6] Fotso H, Feiguin A, Awschalom D and Dobrovitski V 2016 *Phys. Rev. Lett.* **116** 033603
[7] Fotso H and Dobrovitski V 2017 *Phys. Rev.* B **95** 214301
[8] Fotso H 2018 *J. Phys. B: At. Mol. Opt. Phys.* **52** 025501
[9] Lukin D M *et al* 2020 *npj Quantum Inf.* **6** 80
[10] Fotso H F 2019 *Phys. Rev.* B **100** 094309
[11] Joas T, Waeber A M, Braunbeck G and Reinhard F 2017 *Nat. Commun.* **8** 964
[12] Alicki R and Fannes M 2013 *Phys. Rev.* E **87** 042123
[13] Niu Z, Wu Y, Wang Y, Rong X and Du J 2024 *Phys. Rev. Lett.* **133** 180401
[14] Hovhannisyan K V, Perarnau-Llobet M, Huber M and Acín A 2013 *Phys. Rev. Lett.* **111** 240401
[15] Perarnau-Llobet M, Hovhannisyan K V, Huber M, Skrzypczyk P, Brunner N and Acín A 2015 *Phys. Rev.* X **5** 041011
[16] Giorgi G L and Campbell S 2015 *J. Phys. B: At. Mol. Opt. Phys.* **48** 035501
[17] Gyhm J-Y and Fischer U R 2024 *AVS Quantum Sci.* **6** 012001
[18] Ferraro D, Campisi M, Andolina G M, Pellegrini V and Polini M 2018 *Phys. Rev. Lett.* **120** 117702
[19] Santos A C, Çakmak B, Campbell S and Zinner N T 2019 *Phys. Rev.* E **100** 032107
[20] Rosa D, Rossini D, Andolina G M, Polini M and Carrega M 2020 *J. High Energy Phys.* **2020** 1
[21] Arjmandi M B, Mohammadi H and Santos A C 2022 *Phys. Rev.* E **105** 054115
[22] Hu C-K *et al* 2022 *Quantum Sci. Technol.* **7** 045018
[23] Salvia R, Perarnau-Llobet M, Haack G, Brunner N and Nimmrichter S 2023 *Phys. Rev. Res.* **5** 013155
[24] Lu Z-G, Tian G, Lü X-Y and Shang C 2024 arXiv:2405.03675
[25] Gherardini S, Campaioli F, Caruso F and Binder F C 2020 *Phys. Rev. Res.* **2** 013095
[26] Mitchison M T, Goold J and Prior J 2021 *Quantum* **5** 500
[27] Yao Y and Shao X 2022 *Phys. Rev.* E **106** 014138
[28] Gyhm J-Y, Šafránek D and Rosa D 2022 *Phys. Rev. Lett.* **128** 140501
[29] Mazzoncini F, Cavina V, Andolina G M, Erdman P A and Giovannetti V 2023 *Phys. Rev.* A **107** 032218
[30] Cohen-Tannoudji C, Dupont-Roc J and Grynberg G 1998 *Atom-Photon Interactions: Basic Processes and Applications* (Wiley)
[31] Breuer H-P and Petruccione F 2002 *The Theory of Open Quantum Systems* (Oxford University Press)
[32] Allahverdyan A E, Balian R and Nieuwenhuizen T M 2004 *Europhys. Lett.* **67** 565
[33] Francica G, Binder F C, Guarnieri G, Mitchison M T, Goold J and Plastina F 2020 *Phys. Rev. Lett.* **125** 180603
[34] Çakmak B 2020 *Phys. Rev.* E **102** 042111
[35] Shi H-L, Ding S, Wan Q-K, Wang X-H and Yang W-L 2022 *Phys. Rev. Lett.* **129** 130602
[36] Baumgratz T, Cramer M and Plenio M B 2014 *Phys. Rev. Lett.* **113** 140401